SUPPORTING INFORMATION

2-Hydroxyisoquinoline-1,3(2*H*,4*H*)-diones (HIDs), novel inhibitors of HIV integrase with a high barrier to resistance

Belete A. Desimmie, Jonas Demeulemeester, Virginie Suchaud, Oliver Taltynov, Muriel Billamboz, Cedric Lion, Fabrice Bailly, Sergei V. Strelkov, Zeger Debyser, Philippe Cotelle, Frauke Christ

SUPPORTING FIGURES

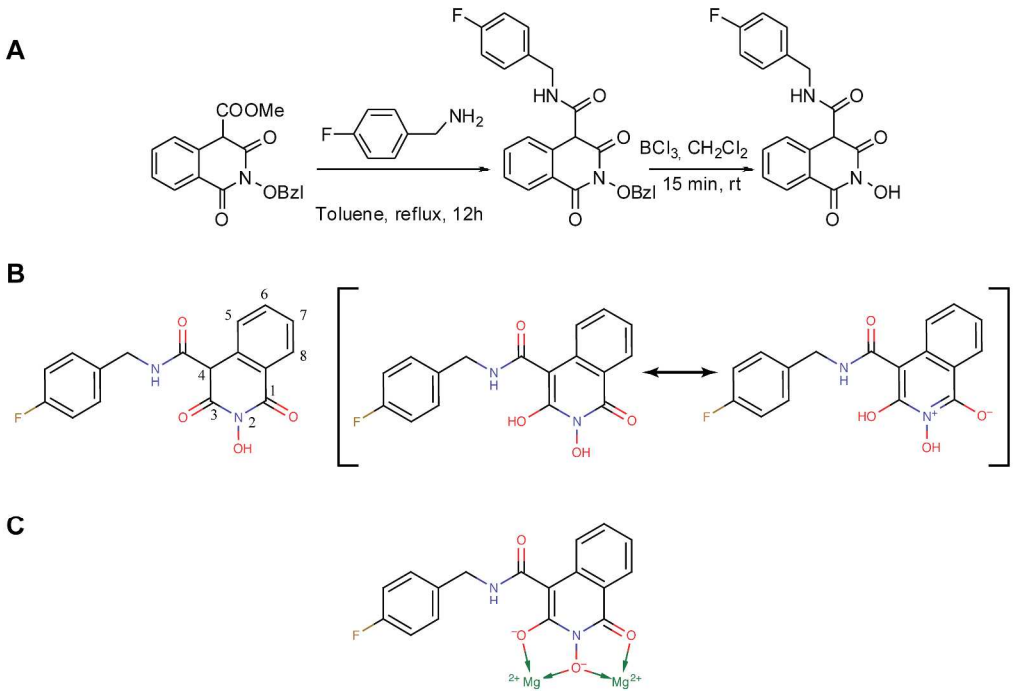

Figure S1: Synthesis scheme and possible tautomers of MB-76. (A) Synthesis of MB-76. (B) MB-76 with the 2-hydroxyisoquinoline-1,3(2*H*, 4*H*)-dione scaffold numbering is shown. The compound readily enolizes upon magnesium complexation to give the middle Lewis structure, which has an aromatic resonance contributor depicted on the right. (C) The MB-76 dianion likely represents the form in which the compound is bound to the retroviral integrase active site, possibly with contributions from other resonance structures.

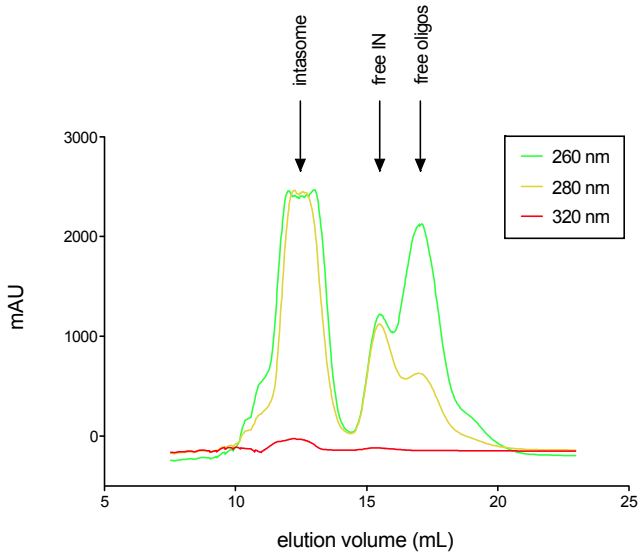

Figure S2. Gel filtration chromatography after PFV intasome assembly. A representative chromatogram is shown from a PFV intasome assembly. Absorbance (mAU: milli-absorbance units) at 260, 280 and 320 nm is shown in order to distinguish protein, DNA and protein-DNA complexes. The assembled intasome readily separates from free integrase and unbound LTR oligonucleotides. Intasome-containing fractions were pooled and proceeded to crystallography or enzymatic assays. The noise mainly at the top of the intasome peak results from the high absorbance (at 260–280 nm) of the sample due to the relatively high concentrations of intasome present.

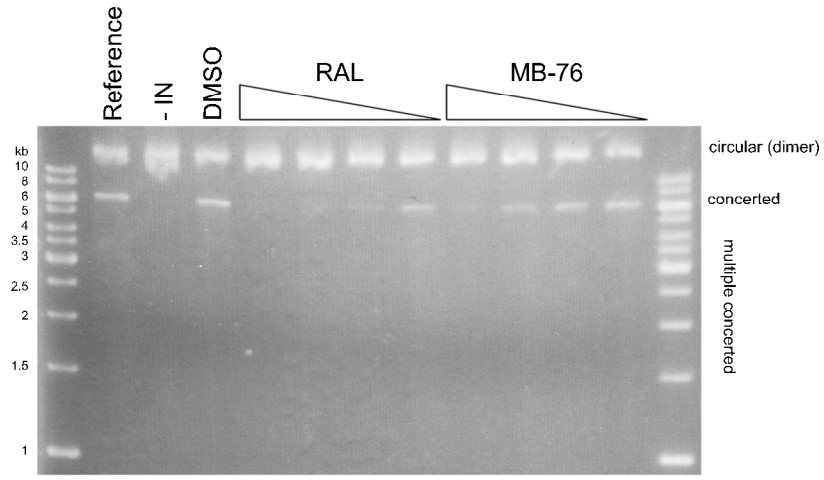

Figure S3. Inhibition of PFV intasome ST by MB-76. Assembled PFV intasome was incubated with buffer, DMSO, RAL or MB-76, after which a peGFP plasmid was added. Resulting DNA was separated on a 1% agarose gel and visualized through ethidium bromide staining. As a result of concerted integration of the intasome oligonucleotides into the plasmid, a novel additional ± 6 kb band appears, representing the open circular form of the plasmid. A light smear can be seen below this band, originating from multiple concerted integrations into single plasmids. The original ± 12 kb band is likely a plasmid dimer. RAL and MB-76 were added at 1000, 200, 40 and 8 nM concentrations. Both compounds inhibit the PFV intasome ST reaction. The DMSO control contained 0.4% (v/v) DMSO, corresponding to the maximal DMSO amount added with the compounds. The reference control contains only intasome, peGFP and buffer, whereas in the –IN control, no intasome was added.

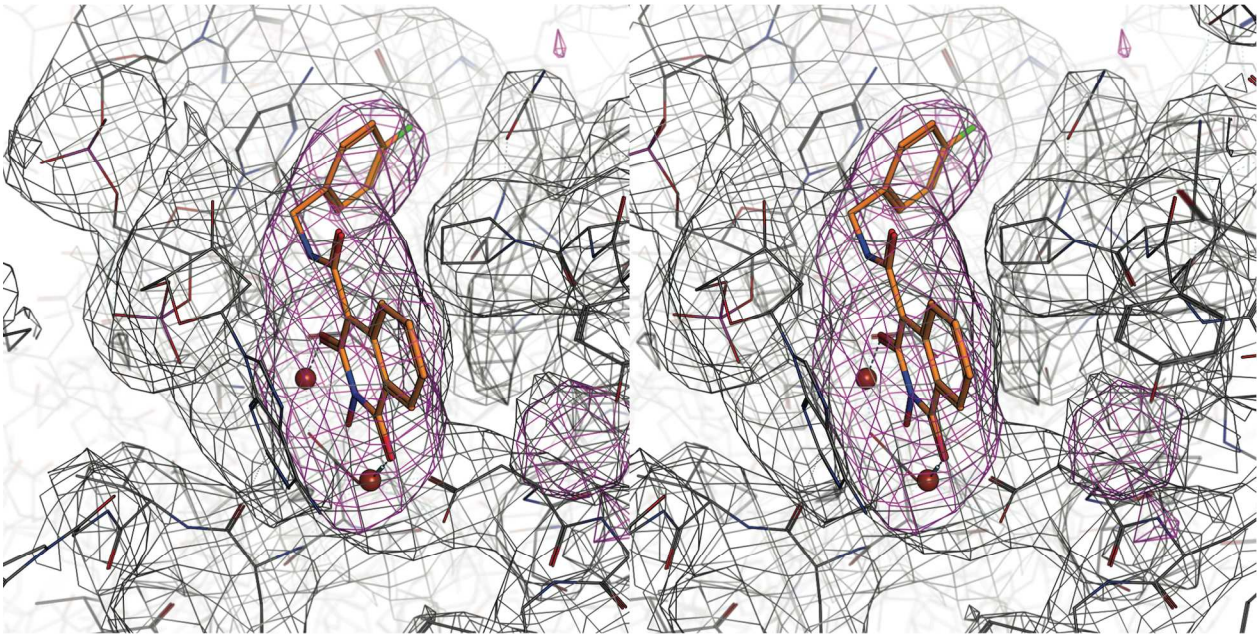

Figure S4. Final and omit electron density maps of the PFV intasome MB-76 co-crystal structure. Wall-eye stereo image showing electron density in the active site of the PFV intasome bound by HID MB-76. The protein/DNA is shown in lines and colored by atom (grey carbons), MB-76 is rendered with sticks (orange carbons) and Mg^{2+} ions are depicted as brown spheres. The final $2F_o$-F_c electron density map is contoured at 1σ and colored grey. An F_o-F_c omit map (where MB-76 and the two active site Mg^{2+} ions were left out from the model during refinement) is rendered as well and contoured in magenta at 5σ. The omit map strongly supports the presence of MB-76 in the active site of the complex. The 3' adenosine base can be seen stacking against against the MB-76 HID core. The small electron density blob present to the right of MB-76 is likely due to the presence of a sulfate ion, as also observed at this position in the PFV intasome co-crystal structures with XZ-259 and analogs.

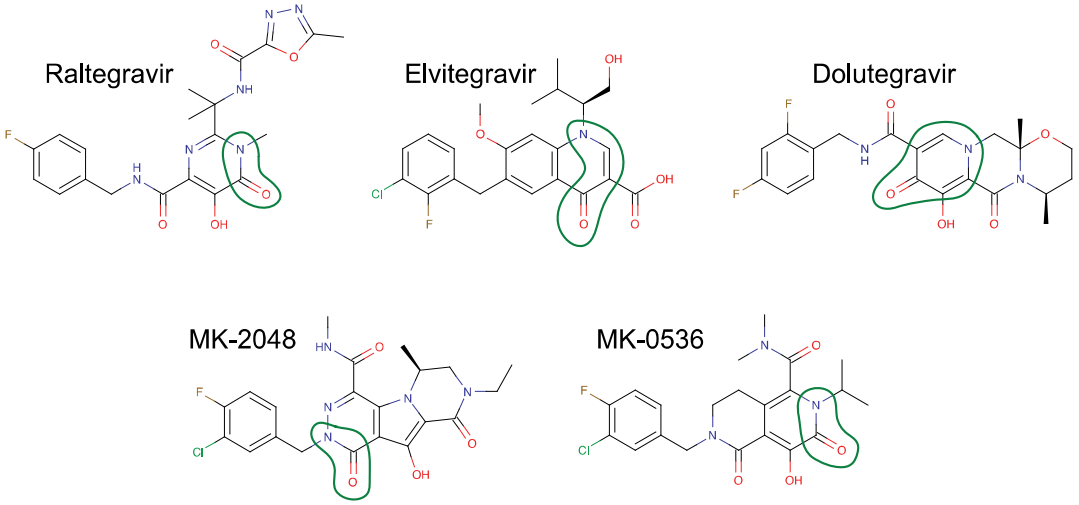

Figure S5. Potent first- and second-generation INSTIs. From top left to bottom right: raltegravir (RAL, MK-0518), elvitegravir (ELV, GS-9137), dolutegravir (DTG, S/GSK1349572), MK-2048, MK-0536. All compounds contain a chelating oxo-group in the α- or γ-position (conjugated, encircled in green) to a lone electron pair of a nitrogen atom (2/4-oxo-pyridine/pyrimidine or 3-oxo-pyridazine) Delocalization of this lone pair in the heterocycle gives an aromatic Lewis structure with a formal negative charge on the chelating oxygen (and a positive charge on the nitrogen). This motif may contribute to INSTI potency.

SUPPORTING TABLES

Table S1: X-ray diffraction data collection and structure refinement statistics. Numbers between parentheses denote the highest resolution shell. Numbers between square brackets indicate the range.

Data collection	
Space group	$P4_12_12$
Unit cell dimensions	
a, b, c (Å)	159.07, 159.07, 123.82
α, β, γ (°)	90, 90, 90
Resolution (Å)	51-3.40 (3.58–3.40)
No. of reflections	21,025
R_{merge}	0.086 (0.611)
$I/\sigma I$	10.0 (2.2)
Completeness (%)	95.1 (96.9)
Redundancy	4.5 (4.3)
Refinement	
Rwork/Rfree	0.18/0.23
No. of atoms	
Protein/DNA	5107
Ligand	24
Glycerol/1,6-hexanediol/ions	46
Mean isotropic B-factor (Å^2)	
Protein/DNA	115
Ligand	82
RMSD	
Bond lengths (Å)	0.025
Bond angles (°)	2.123

Table S2: Quantumchemical analysis of various INSTIs.

Compound	q_1	q_2	q_3	f_{O1}^-	f_{O2}^-	f_{O3}^-	polarizability
RAL	-0.63218	-0.66925	-0.63932	0.04144	0.30036	0.08269	361.41
ELV	-0.57734	-0.71757	-0.79321	0.09185	0.42756	0.15584	327.33
DTG	-0.65846	-0.65603	-0.60980	0.09234	0.27909	0.06689	304.92
MK-2048	-0.63883	-0.67811	-0.65934	0.97445	0.21242	0.08445	374.92
MB-76	-0.76327	-0.63493	-0.74643	0.04834	0.34060	0.14358	308.42

Density Functional Theory (DFT)/B3LYP calculations with the 6-311++G(d,p) basis set were performed. In order to provide insight into the electronic structure of these INSTIs, Natural Bond Orbital (NBO) and Natural Population Analyses (NPA) were performed. Numbering of the chelating oxygen atoms starts with the one most close to the halobenzyl group and proceeds outward from there. Columns 2–5 show natural partial charges on the three chelating oxygens (q_1, q_2 and q_3), which are most relevant for electrostatically controlled reactions associated with hard Lewis acids/bases. Columns 6–9 contain the condensed to atom Fukui indices f_{O1}^-, f_{O2}^-, f_{O3}^- for these oxygens. These are measures for their nucleophilicity in electron transfer reactions involving the frontier molecular orbitals, and represent the indices of choice mainly for soft Lewis acids/bases. The last column contains the calculated isotropic polarizability of the molecules.

Table S3: Inhibition of different members of the cytochrome P450 (CYP450) mixed-function oxidase system by MB-76 and reference compounds.

compound		CYP1A2	CYP2C9	CYP2C19	CYP2D6	CYP3A4
MB-76	% inhibition at 10 µM	**5.2±0.7**	**6.4±0.7**	**18±0.1**	**6.6±3.6**	**35.9±1.7**
Furafyline	IC_{50} [µM]	**1.4**	n.d.[a]	n.d.	n.d.	n.d.
Sulfaphenazole	IC_{50} [µM]	n.d.	**0.18**	n.d.	n.d.	n.d.
Tranylcypromine	IC_{50} [µM]	n.d.	n.d.	**3.1**	n.d.	n.d.
Quinidine	IC_{50} [µM]	n.d.	n.d.	n.d.	**0.017**	n.d.
Ketoconazole	IC_{50} [µM]	n.d.	n.d.	n.d.	n.d.	**0.28**

[a] not determined

Table S4: Detailed analysis of in vitro toxicity of MB-76 and Cerivastatin

assay	compound	1 µM	30 µM	100 µM	IC_{50} [µM][f]
Cytotox (cell number) [a]	MB-76	**-22.8±9.6**	**25.7±5.6**	**16.0±10.6**	n.d.
	Cerivastatin	n.d.[g]	n.d.	n.d.	**0.96**
Intracellular free calcium [b]	MB-76	**-1.7±0.45**	**9.57±1.2**	**29.9±5.8**	n.d.
	Cerivastatin	n.d.	n.d.	n.d.	**0.34**
Nuclear size [c]	MB-76	**-1.0±2.8**	**13.1±4.0**	**18.7±1.4**	n.d.
	Cerivastatin	n.d.	n.d.	n.d.	**0.13**
Membrane permeability [d]	MB-76	**-0.5±1.6**	**20.3±2.7**	**41.2±6.3**	n.d.
	Cerivastatin	n.d.	n.d.	n.d.	**0.80**
Mitochondrial membrane potential [e]	MB-76	**11.8±0.8**	**-21.2±3.4**	**6.3±2.9**	n.d.
	Cerivastatin	n.d.	n.d.	n.d.	**0.6**

[a] % reduction relative to untreated control; [b] % increase relative to untreated control; [c] % reduction relative to untreated control; [d] %increase relative to untreated control; [e] % reduction relative to untreated control; [f] % concentration required to inhibit a–e; [g] not determined.

Table S5: Analysis of cardiac toxicity of MB-76 and the reference compound E-4031 (hERG automated patch-clamp)

compound	0.1 μM	1 μM	10 μM	IC_{50}[μM]
MB-76	**3.4±2.5** [a]	**10.6±1.2**	**13.3±1.3**	n.d. [b]
E-4031	n.d.	n.d.	n.d.	**0.024**

[a] % inhibition of tail current. [b] not determined

SUPPORTING METHODS

Synthesis of MB-76. MB-76 was synthesized in two steps from the known methyl 2-(benzyloxy)-1,3-dioxo-1,2,3,4 tetrahydroisoquinoline-4-carboxylate (*1*). The first step was the reaction of the methyl ester with 4-fluorobenzylamine in refluxing toluene. In a second step, the O-benzyl protection was removed using boron trichloride in dichloromethane giving MB-76 in 59% overall yield (Fig. S1A).

Cell culture. HeLaP4 cells, obtained from the NIH Reagent Program, were grown in Dulbecco's modified Eagle's medium (DMEM) (Gibco-BRL) supplemented with 10% fetal calf serum (FCS) (International Medical), penicillin/streptomycin (100 µg/ml and 100 U/ml, Gibco-BRL) and geneticin (0.5 mg/ml, Gibco-BRL) (further referred to as DMEM-complete). Cells were incubated at 37°C and 5% CO_2 in a humidified atmosphere. MT-4 cells were obtained through the AIDS Research and Reference Reagent Program, Division of AIDS, NIAID, NIH. The cells were grown in RPMI 1640 supplemented with 10% FCS and 20 µg/ml gentamicin (RPMI-complete). To prepare human monocyte derived macrophages (MDM) peripheral blood mononuclear cells (PBMCs) were purified from fresh buffy coats using Lymphoprep (Axis-Shield) as described in the manufacturer's protocol. Subsequently human monocytes were isolated from the PBMCs through depletion of non-monocytes by MACS Cell Separation Columns (Milteny Biotech).

Virus strains. The origins of HIV-1 strains, IIIB and NL4.3 (*2*, *3*), HIV-2 strains, ROD and EHO (*4*, *5*), and simian immunodeficiency virus strain MAC_{251} (*6*) have been described previously. The R5 BaL was obtained through the NIH AIDS Research and Reference Reagent Program, Division of AIDS, NIAID.

Expression and purification of recombinant proteins. His_6-tagged HIV-1 integrase was purified as described previously (*7*). Recombinant PFV integrase was purified as described by Valkov *et al*. and Hare *et al*. with small modifications (*8*, *9*).

Integrase assays. The HIV-1 IN enzymatic integration reactions were carried out with minor modifications as described previously (*7*). To determine the susceptibility of the HIV-1 IN enzyme to different compounds, we used an enzyme-linked immunosorbent assay (ELISA) (adapted from (*10*)). The overall integration assay uses an oligonucleotide substrate for which one oligonucleotide (5'-ACTGCTAGAGATTTTCCACACTGACTAAAAGGGTC-3') is labeled with biotin at the 3' end and the other oligonucleotide (5'-GACCCTTTTAGTCAGTGTGGAAAATCTCTAGCAGT-3') is labeled with digoxigenin at the 5' end. For the strand transfer assay, a precleaved oligonucleotide substrate (the second oligonucleotide lacks GT at the 3' end) was used. The IN enzyme was diluted in 750 mM NaCl, 10 mM Tris (pH 7.6), 10% glycerol and 1 mM β-mercaptoethanol. To perform the reaction, 4 µl of diluted IN (corresponding to a concentration of 1.6 µM) and 4 µl of annealed oligonucleotides (7 nM) were added in a final reaction volume of 40 µl containing 10 mM $MgCl_2$, 5 mM dithiothreitol, 20 mM HEPES (pH 7.5), 5% polyethyleneglycol 8000, and 15% dimethyl sulfoxide. As such, the final concentration of IN in this assay was 160 nM. The reaction was carried out for 1h at 37°C. Reaction products were denatured with 30 mM NaOH and detected by ELISA on avidin-coated plates. Inhibition of 3'processing activity was measured in a classical cleavage assay with detection of products by denaturating gel electrophoresis was performed as described previously (*10*). Briefly, 0.2 pmol of the radioactive labeled oligonucleotide substrate (INT1, ^{32}P-5' TGTGGAAAATCTCTAGCAGT 3'; INT2, 5'ACTGCTAGAGATTTTCCACA 3') and 10 nmol IN in a final volume of 10 µl was incubated for 1h at 37°C. The final reaction

mixture contained 20 mM HEPES pH 7.5, 5 mM DTT, 10 mM $MgCl_2$, 0.5% (v/v) polyethylene glycol 8000 and 15% DMSO. IN was diluted in 750 mM NaCl, 10 mM Tris pH 7.6, 10% glycerol and 1 mM β-mercaptoethanol. The reactions were stopped by the addition of formamide loading buffer (95% formamide, 0.1% xylene cyanol, 0.1% bromophenol blue and 0.1% sodium dodecyl sulfate). Samples were loaded on a 15% denaturating polyacrylamide/urea gel. The extent of 3'-processing or DNA strand transfer was measured based on the respective amounts of -2 bands or strand transfer products relative to the intensity of the total radioactivity present in the lane. These data were determined using the OptiQuant Acquisition and Analysis software (Perkin Elmer Corporate).

Strand transfer assays with PFV intasome were performed as previously described (*8*, *9*) with minor modifications. In short, 30 nM PFV intasome was incubated for 60 min with 300 ng pEGFP-ΔPWWP plasmid in buffer containing 125 mM NaCl, 5 mM $MgCl_2$, 10 mM DTT, 4 μM $ZnCl_2$ and 25 mM Bis-Tris propane. Next, loading dye was added, the samples were separated on a 1% (w/v) agarose gel and visualized after ethidium bromide staining.

Intasome assembly and X-ray crystallography. Both were performed as previously described with minor modifications (*8*, *11*). X-ray diffraction data were collected on the PROXIMA 1 beamline at SOLEIL (Saint Aubin, France) and integrated with Mosflm (*12*) (Table S1). The integrated reflections were scaled and merged with Scala (CCP4 suite (*13*)). The previously published structure of the PFV intasome with Mg^{2+} and DTG (PDB ID 3S3M, 2.5Å resolution (*14*)) served as a starting model which was refined using PHENIX (*15*). MIFit was used to generate the ligand restraints (*16*).

Drug susceptibility assays. The inhibitory effect of antiviral drugs on the HIV-induced cytopathic effect (CPE) in MT-4 cell culture was determined by the MTT-assay (*17*). The assay is based on the reduction of the yellow colored 3-(4,5-dimethylthiazol-2-yl)-2,5-diphenyltetrazolium bromide (MTT) by mitochondrial dehydrogenase of metabolically active cells to a blue formazan derivative, which can be measured spectrophotometrically. The 50% cell culture infective dose of the HIV strains was determined by titration of the virus stock using MT-4 cells. For the drug susceptibility assays, MT-4 cells were infected with 100 to 300 50% cell culture infective doses ($CCID_{50}$) of the HIV strains in the presence of five-fold serial dilutions of the antiviral drugs. The concentration of the compound achieving 50% protection against the CPE of HIV, which is defined as the 50% effective concentration (IC_{50}), was determined. The concentration of the compound killing 50% of the MT-4 cells, which is defined as the 50% cytotoxic concentration (CC_{50}), was determined as well. Infections of human PBMCs were performed with 200,000 cells per well in 96-well plates in RPMI-complete. MB-76 and reference compounds were added at different concentrations and toxicity was monitored. After 6 days of infection replication was evaluated by p24 measurements in the supernatant.

References

1. Billamboz, M., Bailly, F., and Cotelle, P. (2009) Facile synthesis of 4□alkoxycarbonylisoquinoline□1, 3□diones and 5□alkoxycarbonyl□2□benzazepine□1, 3□diones via a mild alkaline cyclization, *Journal of Heterocyclic Chemistry*, Wiley Online Library *46*, 392–398.
2. Adachi, A., Gendelman, H. E., Koenig, S., Folks, T., Willey, R., Rabson, A., and Martin, M. A. (1986) Production of acquired immunodeficiency syndrome-associated retrovirus in human and nonhuman cells transfected with an infectious molecular clone., *J Virol 59*,

284–291.

3. Popovic, M., Sarngadharan, M. G., Read, E., and Gallo, R. C. (1984) Detection, isolation, and continuous production of cytopathic retroviruses (HTLV-III) from patients with AIDS and pre-AIDS., *Science 224*, 497–500.
4. Barré-Sinoussi, F., Chermann, J. C., Rey, F., Nugeyre, M. T., Chamaret, S., Gruest, J., Dauguet, C., Axler-Blin, C., Vézinet-Brun, F., Rouzioux, C., Rozenbaum, W., and Montagnier, L. (1983) Isolation of a T-lymphotropic retrovirus from a patient at risk for acquired immune deficiency syndrome (AIDS)., *Science 220*, 868–871.
5. Rey, M. A., Krust, B., Laurent, A. G., Guetard, D., Montagnier, L., and Hovanessian, A. G. (1989) Characterization of an HIV-2-related virus with a smaller sized extracellular envelope glycoprotein., *Virology 173*, 258–267.
6. Daniel, M., Letvin, N., King, N., Kannagi, M., Sehgal, P., Hunt, R., Kanki, P., Essex, M., and Desrosiers, R. (1985) Isolation of T-cell tropic HTLV-III-like retrovirus from macaques, *Science (New York, NY) 228*, 1201–1204.
7. Busschots, K., Vercammen, J., Emiliani, S., Benarous, R., Engelborghs, Y., Christ, F., and Debyser, Z. (2005) The interaction of LEDGF/p75 with integrase is lentivirus-specific and promotes DNA binding, *J Biol Chem*, ASBMB *280*, 17841–17847.
8. Hare, S., Gupta, S. S., Valkov, E., Engelman, A., and Cherepanov, P. (2010) Retroviral intasome assembly and inhibition of DNA strand transfer, *Nature 464*, 232–236.
9. Valkov, E., Gupta, S. S., Hare, S., Helander, A., Roversi, P., McClure, M., and Cherepanov, P. (2009) Functional and structural characterization of the integrase from the prototype foamy virus., *Nucleic Acids Res 37*, 243–255.
10. Debyser, Z., Cherepanov, P., Pluymers, W., and De Clercq, E. (2001) Assays for the evaluation of HIV-1 integrase inhibitors., *Methods Mol Biol 160*, 139–155.

11. Hare, S., Vos, A. M., Clayton, R. F., Thuring, J. W., Cummings, M. D., and Cherepanov, P. (2010) Molecular mechanisms of retroviral integrase inhibition and the evolution of viral resistance, *Proc Natl Acad Sci USA 107*, 20057–20062.

12. Leslie, A. G. W., and Powell, H. R. (2007) Processing diffraction data with MOSFLM, *Evolving Methods for Macromolecular Crystallography*, Springer 41–51.

13. Winn, M. D., Ballard, C. C., Cowtan, K. D., Dodson, E. J., Emsley, P., Evans, P. R., Keegan, R. M., Krissinel, E. B., Leslie, A. G. W., McCoy, A., McNicholas, S. J., Murshudov, G. N., Pannu, N. S., Potterton, E. A., Powell, H. R., Read, R. J., Vagin, A., and Wilson, K. S. (2011) Overview of the CCP4 suite and current developments., *Acta Crystallogr D Biol Crystallogr 67*, 235–242.

14. Hare, S., Smith, S. J., Métifiot, M., Jaxa-Chamiec, A., Pommier, Y., Hughes, S. H., and Cherepanov, P. (2011) Structural and functional analyses of the second-generation integrase strand transfer inhibitor dolutegravir (S/GSK1349572)., *Mol Pharmacol 80*, 565–572.

15. Adams, P. D., Afonine, P. V., Bunkóczi, G., Chen, V. B., Davis, I. W., Echols, N., Headd, J. J., Hung, L.-W., Kapral, G. J., Grosse-Kunstleve, R. W., McCoy, A. J., Moriarty, N. W., Oeffner, R., Read, R. J., Richardson, D. C., Richardson, J. S., Terwilliger, T. C., and Zwart, P. H. (2010) PHENIX: a comprehensive Python-based system for macromolecular structure solution., *Acta Crystallogr D Biol Crystallogr 66*, 213–221.

16. McRee, D. E. (2004) Differential evolution for protein crystallographic optimizations., *Acta Crystallogr D Biol Crystallogr 60*, 2276–2279.

17. Pauwels, R., Balzarini, J., Baba, M., Snoeck, R., Schols, D., Herdewijn, P., Desmyter, J., and De Clercq, E. (1988) Rapid and automated tetrazolium-based colorimetric assay for the detection of anti-HIV compounds., *J Virol Methods 20*, 309–321.